Journal of Contaminant Hydrology 196 (2017) 10–20

Contents lists available at ScienceDirect

Journal of Contaminant Hydrology

journal homepage: www.elsevier.com/locate/jconhyd

Temperature dependency of virus and nanoparticle transport and retention in saturated porous media

Salini Sasidharan [a,b,c,*], Saeed Torkzaban [a], Scott A. Bradford [d], Peter G. Cook [b,c], Vadakattu V.S.R. Gupta [e]

[a] CSIRO Land and Water, Glen Osmond, SA 5064, Australia
[b] National Centre for Groundwater Research and Training, Adelaide, SA 5001, Australia
[c] Flinders University, Bedford Park, Adelaide, SA 5042, Australia
[d] USDA, ARS, Salinity Laboratory, Riverside, CA 92507, United States
[e] CSIRO Agriculture, Glen Osmond, SA 5064, Australia

ARTICLE INFO

Article history:
Received 8 September 2016
Received in revised form 16 November 2016
Accepted 27 November 2016
Available online 5 December 2016

Keywords:
Temperature
Virus
Nanoparticle
Retention
Surface roughness
XDLVO theory

ABSTRACT

The influence of temperature on virus (PRD1 and ΦX174) and carboxyl-modified latex nanoparticle (50 and 100 nm) attachment was examined in sand-packed columns under various physiochemical conditions. When the solution ionic strength (IS) equaled 10 and 30 mM, the attachment rate coefficient (k_{att}) increased up to 109% ($p < 0.0002$) and the percentage of the sand surface area that contributed to attachment (S_f) increased up to 160% ($p < 0.002$) when the temperature was increased from 4 to 20 °C. Temperature effects at IS = 10 and 30 mM were also dependent on the system hydrodynamics; i.e., enhanced retention at a lower pore water velocity (0.1 m/day). Conversely, this same temperature increase had a negligible influence on k_{att} and S_f values when IS was 1 mM or >50 mM. An explanation for these observations was obtained from extended interaction energy calculations that considered nanoscale roughness and chemical heterogeneity on the sand surface. Interaction energy calculations demonstrated that the energy barrier to attachment in the primary minimum ($\Delta\Phi_a$) decreased with increasing IS, chemical heterogeneity, and temperature, especially in the presence of small amounts of nanoscale roughness (e.g., roughness fraction of 0.05 and height of 20 nm in the zone of influence). Temperature had a negligible effect on k_{att} and S_f when the IS = 1 mM because of the large energy barrier, and at IS = 50 mM because of the absence of an energy barrier. Conversely, temperature had a large influence on k_{att} and S_f when the IS was 10 and 30 mM because of the presence of a small $\Delta\Phi_a$ on sand with nanoscale roughness and a chemical (positive zeta potential) heterogeneity. This has large implications for setting parameters for the accurate modeling and transport prediction of virus and nanoparticle contaminants in ground water systems.

1. Introduction

Groundwater may become contaminated with enteric pathogenic viruses from contaminated recharge water sources, such as infiltration beneath septic tanks, leaking sewer pipes, and managed aquifer recharge with treated wastewater and urban stormwater (Da Silva et al., 2011; Torkzaban et al., 2006; You et al., 2005). Additionally, the increasing use of nanotechnology in a wide range of applications and products will inevitably result in the release of engineered nanoparticles into the subsurface environment (Torkzaban et al., 2013; Wiesner et al., 2006). An understanding and ability to predict the fate and transport of viruses and nanoparticles (NPs) in soils and aquifers are therefore very important for protection of human and environmental health. During passage through porous media, various physicochemical and biological factors influence the attachment of viruses and NPs to solid surfaces, which in turn affects their transport in the subsurface environment. Some of these factors include flow velocity (Hijnen et al., 2005), type of virus or NP (Chu et al., 2001; Fang et al., 2013), temperature (Bradford et al., 2006; Castro and Tufenkji, 2007; Chrysikopoulos and Aravantinou, 2014; Gallardo-Moreno et al., 2003; García-García et al., 2006; Kim and Walker, 2009; McCaulou et al., 1995), solution chemistry (e.g., ionic strength, pH, ion type) (Gutierrez et al., 2010; Kim et al., 2009), solid surface roughness (Bradford and Torkzaban, 2013; Torkzaban and Bradford, 2016) and chemical heterogeneities (Johnson et al., 1996). A few studies observed an increased adsorption for microlatex colloids, bacteria, and viruses to several adsorbents with temperature and attributed to factors such as an increase in viscosity of the medium, enhanced bacterial polymer formation, viral protein folding, protein attachment, and virus hydrophobicity, and higher inactivation of bacteria/virus at a higher temperature (Bales et al., 1991; Bellamy et al., 1985; Fletcher, 1977; Hendricks et al., 1979; McCaulou et al., 1995;

Abbreviations: IS, ionic strength; XDLVO, Extended Derjaguin-Landau-Verwey-Overbeek; NPs, nanoparticles; CFT, colloid filtration theory; EDL, electrostatic double layer interaction; vdW, van der Waals interaction; PFU, plaque forming unit; BTC, breakthrough concentrations; EM, electrophoretic mobility; PV, pore volumes.

* Corresponding author at: CSIRO Land and Water, Glen Osmond, SA 5064, Australia.
E-mail address: salini.sasidharan@flinders.edu.au (S. Sasidharan).

http://dx.doi.org/10.1016/j.jconhyd.2016.11.004
0169-7722/

Nomenclature

k_{att}	attachment rate coefficient (day^{-1})
S_f	percentage of the sand surface area that contributed to attachment (%)
S_{fT}	theoretical values of S_f
$S_{\max}$	maximum solid phase concentrations of attached latex NPs on site 1 + 2 (N kg^{-1})
C_0	input concentration (N mL^{-1})
C	effluent concentration (N mL^{-1})
C/C_0	relative effluent concentrations
v	pore water velocity (m day^{-1})
A_z	zone of influence on the solid-water-interface (nm^2)
f_r	nanoscale roughness fraction
h_r	roughness height (nm)
f_+	positive zeta potential fraction
ζ_+	positive zeta potential (mV)
Greek symbols	
η	single-collector efficiency
α	attachment efficiency
α_T	theoretical values of α
$\Phi_1{}^0{}_{min}$	depth of the primary energy minimum
$\Phi_{\max}$	height of the energy barrier
$\Delta\Phi_a$	energy barrier to attachment in the primary minimum
$\Phi_2{}^0{}_{\min}$	depth of secondary energy minimum

Zhang et al., 2012). While temperature has been noted to affect transport, little research attention has been given to understanding how the temperature influences the attachment process of viruses and NPs (Chrysikopoulos and Aravantinou, 2014).

Attachment of viruses and NPs to solid surfaces of porous media under saturated conditions is commonly described using colloid filtration theory (CFT). According to this theory, the attachment rate is dependent on the mass transfer rate of particles from the bulk solution to the collector surface (quantified by the single-collector efficiency, η) and subsequent particle-surface interaction (quantified by the attachment sticking efficiency, α) (Schijven and Hassanizadeh, 2000; Tufenkji and Elimelech, 2004). Correlation equations have been developed for calculating η as a function of parameters such as flow velocity, viscosity, temperature, diffusion, and particle size. It is predicted that the value of η, and consequently the attachment rate coefficient (k_{att}), increases with temperature due to an increase in the diffusion coefficient (Schijven and Hassanizadeh, 2000; Tufenkji and Elimelech, 2004; Yao et al., 1971). For example, the value of η increases by about 37% with an increase in temperature from 4 to 20 °C. However, several studies have reported that the value of k_{att} increased with temperature to a much greater extent than η (Kim and Walker, 2009; McCaulou et al., 1995). For example, Kim and Walker (2009) observed that k_{att} for latex microspheres at 25 °C was 173% greater than that at 10 °C. It is, therefore, reasonable to expect that the value of α should also increase with temperature.

The value of α strongly depends on the interaction energy between a particle (e.g., virus and NP) and collector (e.g., sand grain) surface (Shen et al., 2010; Tufenkji and Elimelech, 2004). Extended Derjaguin-Landau-Verwey-Overbeek (XDLVO) theory predicts that the total interaction energy consists of electrostatic double layer (EDL) and van der Waals (vdW) interactions (Derjaguin, 1941; Verwey, 1947), as well as poorly characterized short-range interactions such as Born, Lewis acid-base, and hydration interactions (Van Oss, 1993; Yoon et al., 1997). The depth of secondary energy minimum ($\Phi_2{}^0{}_{\min}$) is very small for NPs (Bhattacharjee et al., 1998). Consequently, the value of α for NPs is mainly controlled by the energy barrier to attachment in the primary minimum ($\Delta\Phi_a$) and the depth of the primary energy minimum ($\Phi_1{}^0{}_{\min}$); the value of $\Delta\Phi_a = \Phi_{\max} - \Phi_2{}^0{}_{\min}$ where $\Phi_{\max}$ is the height of the energy barrier. The attractive vdW energy is expected to increase with temperature, due to an increase in the Hamaker constant with temperature (Yan et al., 2015). The magnitude of the repulsive EDL energy is predicted to slightly decrease with increasing temperature due to the decrease in the dielectric constant of the solution, surface potentials of the particle and solid surfaces, and the inverse Debye length (Adamczyk, 2006; Galisteo et al., 1990; Yan et al., 2015). Consequently, an increase in temperature may enhance particle attachment in the primary minimum by lowering $\Delta\Phi_a$ to levels that allow a nanoparticle to diffuse over the energy barrier. However, XDLVO theory for homogeneous interacting surfaces commonly predicts the existence of a sizable energy barrier against attachment in the primary minimum (e.g., >7 kT, where k is the Boltzmann constant and T is the absolute temperature) under unfavorable chemical conditions typical of fresh groundwater (e.g., ionic strength <10 mM) (Bradford and Kim, 2012; Bradford and Torkzaban, 2013; USGS, 2013). Note that the thermal energy of diffusing particles is considerably less than a few kT with an average of 1.5 kT (Shen et al., 2007). Hence, the energy barrier approach (Bhattacharjee et al., 2000) predicts that a small reduction of $\Delta\Phi_a$ with temperature is unlikely to produce enhanced attachment in the primary minimum when $\Delta\Phi_a$ is large (Bradford et al., 2004). In contrast, a substantial increase in the rate and extent of particle attachment has been experimentally observed when the temperature of the solution was increased by 10 or 20 degrees (Kim and Walker, 2009).

Nanoscale roughness and chemical heterogeneities on grain surfaces have been shown to substantially reduce or eliminate $\Delta\Phi_a$ at some localized locations under a net-unfavorable condition (Bhattacharjee et al., 1998; Shen et al., 2012; Suresh and Walz, 1997; Torkzaban and Bradford, 2016). For example, under low ionic strength (<10 mM) conditions, particle attachment may occur on some localized "favorable" sites that exhibit no repulsion or a shallow energy barrier (a few kT) to attachment in the primary energy minimum (Huang et al., 2009). Therefore, the value of α is proportional to the fraction of the solid surface that is "favorable" for attachment. Indeed, numerous studies have shown that only a small percentage of the surface area of a porous medium is favorable for particle attachment (S_f) under a given chemical condition (Argent et al., 2015; Magal et al., 2011; Sasidharan et al., 2014; Treumann et al., 2014). Therefore, we hypothesize that nanoscale surface roughness and chemical heterogeneity play the main role in enhancing the influence of temperature on NP attachment. An increase in temperature further reduces the magnitude of a shallow $\Delta\Phi_a$ created by nanoscale roughness and chemical heterogeneity, which enables more particles to realize a $\Phi_1{}^0{}_{\min}$ attachment at higher temperature. Thus, it is reasonable to expect that the value of α and thereby, the value of S_f would increase with temperature. However, no systematic theoretical and experimental studies have been conducted to investigate the effect of temperature on the value of S_f.

The objective of this study was to experimentally and theoretically investigate the influence of water temperature, coupled with solution chemistry and flow velocity, on the extent and kinetics of virus and NP attachment in a porous medium. For this purpose, two different biotic (PRD1 and ΦX174 viruses) and abiotic (50 and 100 nm carboxyl-modified latex NPs) nanoparticles were employed in this study. The transport experiments were performed at 4 and 20 °C at various solution ionic strength (IS) and pore water velocities. Values of k_{att} and S_f were determined by parameter fitting to the observed breakthrough concentrations of the NPs. XDLVO calculations between a chemically and physically heterogeneous collector and homogeneous particle were conducted to explain the observed enhanced attachment of the viruses and latex NPs at the higher temperature. Specific solution chemistry conditions were identified when temperature-dependent particle transport is expected. Results from this work provide insight into the underlying mechanisms that control the influence of temperature on particle attachment in porous media and have important implications for determining the potential importance of transients in water temperature on virus and nanoparticle fate and transport in the subsurface environment.

2. Materials and method

2.1. Electrolyte solutions and porous medium

Electrolyte solutions of 1, 10, 30, and 50 mM NaCl were prepared using analytical grade NaCl and Milli-Q water at pH = 5.5–5.8. Ultra-pure quartz sand (Charles B. Chrystal CO., Inc., NY, USA) with size ranging from 125 to 300 μm was employed in transport experiments. This sand was cleaned using an acid wash and boiling procedure described by (Sasidharan et al., 2014). This idealized quartz sand was selected in order to minimize many of the complexities associated with natural soil and aquifer materials such as organic matter, clay, and metal oxides (Castro and Tufenkji, 2007; Chrysikopoulos and Aravantinou, 2012; Kim and Walker, 2009).

2.2. Viruses

Bacteriophage PRD1 and ΦX174 were used in this study. The characteristics of these phages and their production and quantification using the double layer agar (DLA) method are described in our previous study (Sasidharan et al., 2016). The DLA method has a detection limit of around 30 plaque forming unit (PFU) mL^{-1} (ISO 10705-2-2000, 2000). Stock solutions of phages were diluted in each electrolyte solution and equilibrated at the experimental temperature (4 and 20 °C) to obtain an input concentration (C_0) of about 5×10^6 PFU mL^{-1}. The inactivation rate of viruses over a period of 140 h was determined in representative electrolyte solutions at both temperatures and a representative result is given in Fig. S1.

2.3. Latex nanoparticles

Carboxyl-modified latex NPs (Polysciences, Inc.) of two different sizes (50 and 100 nm) were used in this study. The manufacturer reported that the 50 and 100 nm NPs had a concentration of 3.64×10^{14} and 4.55×10^{13} particles mL^{-1}, respectively. Stock solutions of 50 and 100 nm NPs were diluted to obtain a C_0 of 1.1×10^{11} and 2.4×10^{10} particles mL^{-1}, respectively. The aqueous phase concentrations of NPs were determined using a fluorescence spectrophotometer (Synergy HT, BioTek Instruments, Inc., Winooski, VT, USA) and a calibration curve at an excitation and emission wavelength of 441 nm and 486 nm, respectively. The manufacturer reported that the NPs had a density of 1.05 g cm^{-3}. The detection limit for the 50 and 100 nm latex NPs is ~6.5×10^8 and ~4.5×10^8 NPs mL^{-1}, respectively.

2.4. Zeta potential and size measurements

The electrophoretic mobility (EM) of latex NPs, viruses, and crushed quartz (<2 μm) was measured in the electrolyte solutions (1 to 50 mM) using a Zetasizer (Malvern, Zetasizer Nano Series, Nano-ZS). The temperature setup option on the instrument was used to measure the EM at different temperatures. The samples were first equilibrated to the selected temperature (4 and 20 °C) for 10 min and then EM measurements were repeated five times with more than twenty runs per measurement. The Smoluchowski equation (Elimelech et al., 1994) was used to convert the measured EM values to zeta potentials. The changes in fluid properties (viscosity and dielectric constant) at different temperatures were taken into account in these calculations.

The size distribution of viruses and latex NPs in different electrolyte solutions (1 to 50 mM) and temperatures was measured using a dynamic light scattering (DLS) process (Malvern, Zetasizer Nano Series, Nano-ZS). DLS also known as photon correlation spectroscopy measures the translational diffusion coefficient of particles that are subject to Brownian motions and relates this to the size of the particles. The size expressed as the hydrodynamic diameter, is determined by illuminating the particles using a laser and analyzing the intensity fluctuations in the scattered light (Malvern Instruments Ltd, 2004; Sikora et al., 2016).

2.5. Column transport experiments

The column experiments were conducted in temperature-controlled laboratories (4 ± 1 and 20 ± 1 °C). Sterilized polycarbonate columns (1.9 cm inside diameter and 5 cm height) were wet-packed using clean quartz sand while the column was being vibrated. The packed column has a porosity of 0.4. After packing, the column was preconditioned with >10 pore volumes (PV) of a selected electrolyte solution using a syringe pump (Model 22, Harvard Apparatus) at a pore water velocity of 5 m day^{-1}. The columns were equilibrated to the selected temperature (4 and 20 °C) for 12 h before starting the experiment.

A virus (PRD1 and ΦX174) or latex NP (50 and 100 nm) suspension at selected IS (1, 10, 30, and 50 mM Na^+) and temperature (4 or 20 °C) was introduced into the column using a syringe pump at an average pore water velocity of 0.1 or 1 m day^{-1} for 20 PV (Phase 1). This phase was followed by injection of ~10 PV of the particle-free solution at the same IS, temperature, and pore water velocity (Phase 2). The column effluent samples were collected using a Spectra/Chrom® CF-1 Fraction Collector and the concentration of viruses or latex NPs was quantified using methods explained above. The total mass of retained particles during Phases 1 and 2 ($N_{1\,+\,2}$) was determined by calculating the difference between the mass of injected particles into the column in Phase 1 (N_{in}) and the mass of particles that was recovered in the effluent during Phases 1 and 2 (N_{out}). This information was used to calculate the mass percentage of retained particles (PR) in the column in each experiment.

All experiments were duplicated and the statistical differences of mean removal efficiencies were identified by one-way ANOVA. The mean removal efficiencies were separated by Tukey's honestly significant difference (HSD) test ($p < 0.05$). All statistical analyzes were performed using IBM SPSS Statistics for Windows Version 22.0 (IBM SPSS, 2013).

It should mention that retention profiles for viruses and latex NPs were not determined in this study because of significant amounts of irreversible primary minimum attachment, as well as solid phase inactivation for viruses (Bradford et al., 2006; Bradford et al., 2012). The relative importance of surface straining processes on retention and release decreases for smaller particle size and higher solution ionic strengths (Bradford and Torkzaban, 2015).

3. Theoretical calculations

3.1. Breakthrough curve (BTC) simulations

The experimental BTCs for viruses and latex NPs were simulated using the Hydrus-1D model (Simunek et al., 2005). This model allows for advective and dispersive transport, irreversible attachment on site 1, and reversible attachment on site 2. The following aqueous and solid phase mass balance equations were considered in this model:

$$\frac{\partial C}{\partial t} = \lambda v \frac{\partial^2 C}{\partial z^2} - v \frac{\partial C}{\partial z} - r_{att} \tag{1}$$

$$r_{att} = \frac{\rho_b}{\theta}\ \frac{\partial (S_1\ + S_2)}{\partial t} = k_{att1}\psi_1 C + k_{att2}\psi_2 C - \frac{\rho_b}{\theta}\ k_{det2} S_2 \tag{2}$$

where t (T; T denotes units of time) is time, z (L; L denotes units of length) is the direction of mean water flow, C (NL^{-3}; N denotes number) is the number of viruses or latex NPs per unit volume of the aqueous phase, λ (L) is the dispersivity, v (LT^{-1}) is the average pore water velocity, r_{att} (NL^{-3} T^{-1}) is the particle attachment rate to the solid surfaces,

ρ_b (ML^{-3}; M denotes units of mass) is the bulk density, θ is the water content, S_1 and S_2 (NM^{-1}) are the solid phase concentrations of particles (viruses or latex NPs) on site 1 and site 2, respectively, k_{att1} and k_{att2} (T^{-1}) are the attachment rate coefficients for site 1 and site 2, respectively, and k_{det2} (T^{-1}) is the detachment rate coefficient for site 2. The parameters ψ_1*and* $\psi_2$are dimensionless Langmuirian blocking functions that are given as (Adamczyk et al., 2013):

$$\psi_1 = \left(1 - \frac{S_1}{S_{max1}}\right) \qquad \text{and} \qquad \psi_2 = \left(1 - \frac{S_2}{S_{max2}}\right) \tag{3}$$

where S_{max1} and S_{max2} (NM^{-1}) are the maximum solid phase concentrations of attached latex NPs on site 1 and site 2, respectively. As it will be shown, negligible detachment was observed for the latex NPs, and therefore the value of $k_{det2}$was set to zero for the latex NP simulations. Blocking was not observed in the BTCs of viruses. The C_0 of viruses is ~10^5 times smaller than that for the latex NPs. Considering the smaller size and attachment rate for viruses, the time that it takes for viruses to fill S_f will be ~10^5 times longer. Therefore, blocking was neglected for viruses by setting $\psi_1$and $\psi_2$to 1. Solid and liquid inactivation of viruses was found to be negligible over the relatively short duration of these transport experiments (Fig. S1) and therefore, all the removal was attributed to attachment.

The total value of k_{att} and S_{max} for the viruses and latex NPs were defined as $k_{att1} + k_{att2}$ and $S_{max1} + S_{max2}$, respectively. The value of α was calculated from k_{att} using filtration theory as (Schijven and Hassanizadeh, 2000; Yao et al., 1971):

$$\alpha = \frac{2 d_c k_{att}}{3(1-n) v \eta} \tag{4}$$

where n is the porosity (0.4) and d_c (L) is the collector diameter. Many correlations have been developed to predict η (Logan et al., 1995; Ma et al., 2013; Rajagopalan and Tien, 1976; Tufenkji and Elimelech, 2004; Yao et al., 1971). However, some of these correlations predict a η value that is greater than one, which is physically questionable (Ma et al., 2013), when typical groundwater flow conditions are considered (e.g., $v \approx 0.1$ m day^{-1}). Messina et al. (2015) have recently developed a correlation equation for η to overcome this shortcoming. Indeed, calculated values of η were greater than one for both latex NPs and viruses at $v = 0.1$ m day^{-1} when using correlations of (Tufenkji and Elimelech, 2004; Yao et al., 1971). The correlation equation of (Messina et al., 2015) was therefore employed to determine the value of η in this study and values were significantly ($p < 0.008$) different to those calculated using previous correlations (Tufenkji and Elimelech, 2004; Yao et al., 1971).

The value of S_f was calculated from S_{max} as (Kim et al., 2009):

$$S_f = \frac{A_c \rho_b S_{max}}{(1-\gamma) A_s} 100 \tag{5}$$

where A_c ($L^2 N^{-1}$) is the cross sectional area of a particle, A_s (L^{-1}) is the solid surface area per unit volume, and γ is the porosity of a monolayer packing of particles on the solid surface that was set to 0.5 based on information in (Johnson and Elimelech, 1995).

3.2. XDLVO interaction energy calculations

The total interaction energy between homogeneous particle and collector surfaces was determined as:

$$\Phi_{Total} = \Phi_{vdW} + \Phi_{EDL} + \Phi_{BR} \tag{6}$$

where Φ_{Total} (ML^2T^{-2}) is the total interaction energy, Φ_{vdW} (ML^2T^{-2}) is the van der Waals interaction, Φ_{EDL} (ML^2T^{-2}) is the electrostatic double layer interaction, and Φ_{BR} (ML^2T^{-2}) is the interaction due to Born repulsion. The value of Φ_{vdW} was determined from the expression of (Gregory, 1981). The Hamaker constant for each particle-water-quartz system was determined by including the temperature dependency of the refractive index and the dielectric constant as explained in detail by (Yan et al., 2015). The combined Hamaker constant for latex NP-water-quartz was equal to 6.5×10^{-21} at 4 °C and 6.8×10^{-21} J at 20 °C; whereas for virus-water-quartz it was 4.04×10^{-21} J at 4 °C and 4.24×10^{-21} J at 20 °C. The value of Φ_{EDL} was calculated using the Hogg-Healy-Fuerstenau expression (Hogg et al., 1966) with zeta potentials in place of surface potentials. The value of Φ_{BR} was calculated using the approach of (Ruckenstein and Prieve, 1976) by setting the collision diameter at 0.21 nm to achieve a primary minimum depth at 0.157 nm (Van Oss et al., 1988).

Natural solid surfaces like sand grains always contain a wide distribution of physical (roughness) or chemical (e.g., metal oxides) heterogeneities. The interaction energy between a homogenous particle and a heterogeneous collector was calculated by assuming that the zone of influence (A_z) on the solid-water-interface contained nanoscale chemical and roughness heterogeneities. Each A_z was assumed to contain a nanoscale roughness fraction (f_r) of 0.01–0.1 with a height (h_r) of 1–20 nm and a positive zeta potential fraction (f_+) of 0.01–0.1 with a positive zeta potential (ζ_+) of 1–10 mV. Note that the values of heterogeneity parameters used in this study are hypothetical since accurate measurements or characteristics of these parameters are not yet available. However, similar values for the heterogeneity parameters were used in many previous studies (Bradford and Torkzaban, 2015; Torkzaban and Bradford, 2016). The value of interaction energy (Φ) within A_z was subsequently quantified using a linear combination of interaction energies associated with nanoscale heterogeneities and the homogenous surface as explained by (Bradford and Torkzaban, 2015). Theoretical values of α and S_f (α_T and S_{fT}) were calculated as the average of 10,000 A_z realizations using the approach described by (Bradford and Torkzaban, 2015). The contact angles for quartz, ΦX174, latex NPs have been reported to be equal to 0°, 26°, and 36°, respectively (Attinti et al., 2010; Sirivithayapakorn and Keller, 2003; Subrahmanyam et al., 1999). The contribution of hydrophobic interaction is considered to be negligible when the contact angle is <90° (Vogler, 1998), and it was therefore not considered. In addition, many previous studies neglected the hydrophobic interactions for PRD1 in DLVO interactions energy calculation (Ryan et al., 1999; Sadeghi et al., 2011, 2013).

4. Results and discussion

4.1. Interaction energy for homogenous surfaces

Table 1 presents the measured zeta potential values of the viruses, latex NPs, and sand for the various IS and temperature conditions. Zeta potentials of all surfaces were negatively charged at the pH of the experiments (5.5–5.8) and become less negative with increasing IS. Note that the zeta potential values for a given surface and IS were nearly identical (±4 mV) at the two temperature of 4 and 20 °C (Table S1). Hence, an increase in the temperature from 4 to 20 °C did not significantly influence the electrokinetic properties of the viruses, latex NPs, and sand. It is worth mentioning that temperature has been reported to have variable effects on the electrokinetic properties of solid surfaces (Castro and Tufenkji, 2007; García-García et al., 2009; Ishido et al., 1983; Reppert and Morgan, 2003; Rodríguez and Araujo, 2006). A few studies reported that zeta potentials of various materials become more negatively charged with increasing temperature from 4 to 50 °C (0.012–0.5 per °C) (Kim and Walker, 2009; Rodríguez and Araujo, 2006). However, other researchers found that increasing temperature from 4 to 40 °C resulted in a decrease in the magnitude of the zeta potentials (0.16–0.25 per °C) (Dhont and Briels, 2008; Freitas and Müller, 1998; Galisteo et al., 1990). Castro and Tufenkji (2007) reported that the dissociation constant of certain acidic and basic groups can be sensitive to temperature, whereas other functional groups such as –COOH are insensitive to temperature. Variations in the surface functional groups present on the

Table 1
Measured values of zeta potential and calculated values of the energy barrier to attachment in primary minimum ($\Delta\Phi_a = \Phi_{max} - \Phi_2{}^0{}_{min}$) for 50 and 100 nm latex NPs and viruses (ΦX174 and PRD1).

Particle	IS	Zeta potential	Temperature	$\Delta\Phi_a = \Phi_{max} - \Phi_2{}^0{}_{min}$ homogeneous[a]	$\Delta\Phi_a = \Phi_{max} - \Phi_2{}^0{}_{min}$ physically and chemically heterogeneous[b]
	[mM]	[mV ± STDV[c]]	[°C]	[kT ± STDV[c]]	[kT ± STDV[c]]
50 nm (NP)	1	−48 ± 1.5	4	33 ± 0.7	13 ± 0.2
			20	29 ± 0.5	11 ± 0.4
	10	−40 ± 1.7	4	23 ± 0.6	1.0 ± 0.06
			20	20 ± 0.1	0.9 ± 0.03
	30	−35 ± 1.3	4	14 ± 0.1	0.5 ± 0.09
			20	11 ± 0.6	0.4 ± 0.08
	50	−25 ± 0.9	4	2.0 ± 0.07	0.1 ± 0.09
			20	1.1 ± 0.09	0
100 nm (NP)	1	−51 ± 1.4	4	101 ± 0.8	27 ± 0.8
			20	88 ± 0.9	24 ± 0.9
	10	−47 ± 1.8	4	59 ± 0.1	2.6 ± 0.03
			20	50 ± 0.7	2.2 ± 0.02
	30	−40 ± 2.5	4	31 ± 0.8	1.2 ± 0.06
			20	26 ± 0.4	1.0 ± 0.03
	50	−31 ± 2.6	4	6.1 ± 0.05	0.2 ± 0.01
			20	4.0 ± 0.07	0.1 ± 0.03
PRD1 (63 nm)	1	−37 ± 1.7	4	40 ± 0.9	13 ± 0.2
			20	35 ± 0.7	11 ± 0.4
	10	−33 ± 2.2	4	28 ± 0.8	1.3 ± 0.09
			20	24 ± 0.6	1.1 ± 0.07
	50	−20 ± 3.1	4	2.1 ± 0.09	0.1 ± 0.01
			20	2.0 ± 0.02	0.07 ± 0.001
ΦX174 (27 nm)	1	−36 ± 1.6	4	11 ± 0.1	5.3 ± 0.02
			20	10 ± 0.3	5.1 ± 0.01
	10	−30 ± 1.8	4	8.8 ± 0.02	0.5 ± 0.03
			20	7.5 ± 0.01	0.4 ± 0.05
	50	−17 ± 1.7	4	1.3 ± 0.02	0.06 ± 0.001
			20	1.2 ± 0.02	0.04 ± 0.001
Sand	1	−38 ± 2.4			
	10	−27 ± 1.5		NA[d]	NA[d]
	30	−23 ± 1.2			
	50	−15 ± 0.7			

[a] Smooth sand surface.
[b] Physically and chemically heterogeneous sand surface. The physical and chemical heterogeneity parameters used for calculations are $f_r = 0.05$, $h_r = 20$ nm, $f_+ = 0.1$ and $\zeta_+ = 1$ mV.
[c] STDV = standard deviation.
[d] NA = not applicable.

various colloid surfaces may explain the observed discrepancies in zeta potential value with temperature. The average size of the viruses and the latex NPs for the various IS and temperature conditions was very stable; ΦX174 = 27 ± 3.5 nm, PRD1 = 63 ± 3.9 nm, 50 nm latex = 50 ± 3.6, and 100 nm latex = 100 ± 4.9 nm. This data indicates that the colloidal suspensions were not aggregating under the considered experimental conditions. Measured average zeta potentials at both temperatures (Table 1) and average particle sizes were therefore used for subsequent XDLVO calculations.

The interaction energy profile of latex NPs and viruses on approach to a physically and chemically homogeneous quartz surface was calculated using XDLVO theory. The height of the energy barrier to attachment in the primary minimum ($\Delta\Phi_a = \Phi_{max} - \Phi_2{}^0{}_{min}$) is given in Table 1 for all the IS and temperature conditions. As expected, the height of $\Delta\Phi_a$ decreased with increasing IS and decreasing particle size. At IS = 50 mM, the energy barrier is completely eliminated because of the relatively low zeta potentials of the sand and particles. The magnitude of $\Delta\Phi_a$ slightly decreased with increasing temperature when the IS <50 mM due to the increase in the attractive van der Waal interaction; i.e., the Hamaker constant was greater at a higher temperature (Yan et al., 2015) and the electrostatic repulsion was reduced due to the decrease in Debye-length (κ^{-1}) with temperature ($\kappa^{-1} = 3.06$ nm at 4 °C and $\kappa^{-1} = 3.04$ nm at 20 °C). However, a sizable $\Delta\Phi_a$ (>7 kT) was predicted for all particles at both temperatures when IS < 50 mM, which, in principle, should inhibit primary minimum attachment of the particles to sand surfaces (Torkzaban and Bradford, 2016; Tufenkji and Elimelech, 2005). It should be mentioned that the depth of the $\Phi_2{}^0{}_{min}$ was smaller than ~0.5 kT under all conditions (Table S2), indicating that attachment in the $\Phi_2{}^0{}_{min}$ was highly unlikely (Tufenkji and Elimelech, 2005).

4.2. Retention of viruses and latex NPs in column experiments

Fig. 1 shows representative observed and fitted BTCs for PRD1 and ΦX174 when $v = 0.1$ m day^{-1}, IS = 10 and 50 mM, and temperature = 4 and 20 °C. Here, the relative effluent concentrations (C/C_0; where C is the effluent and C_0 is the influent concentration) were plotted on a logarithmic scale as a function of PV. Tables 2 and S3 presents values of mass retained for the viruses (log scale) and replicate experimental results, respectively. The BTCs showed negligible virus retention when the viruses were suspended in 1 mM solution at both temperatures (Table S3). Fig. 1 shows that virus retention dramatically increased with increasing IS at a given temperature. For example, >2 logs (>99%) of the injected viruses were retained in the column when IS was 10 mM. Furthermore, the BTCs exhibited a plateau during the 10 PVs of virus injection, implying that filling of available attachment sites was minimal and, therefore, did not affect the kinetic of the attachment process in these experiments. It is interesting to observe that increasing temperature from 4 to 20 °C did not have much of an effect on the BTCs when the IS was 50 mM. In contrast, the BTCs were dependent on temperature when the IS was 10 mM. Notably, about one log (90%) more virus retention occurred at 20 °C than 4 °C when the IS was 10 mM.

Fitted values of the model parameters (i.e., k_{att1}, k_{att2}, and k_{det2}) and the Pearson's correlation coefficient (R^2) for the two viruses in each experiment are given in Table 2. The low detection limit for viruses (~30 viruses mL^{-1}) facilitated the accurate determination of model

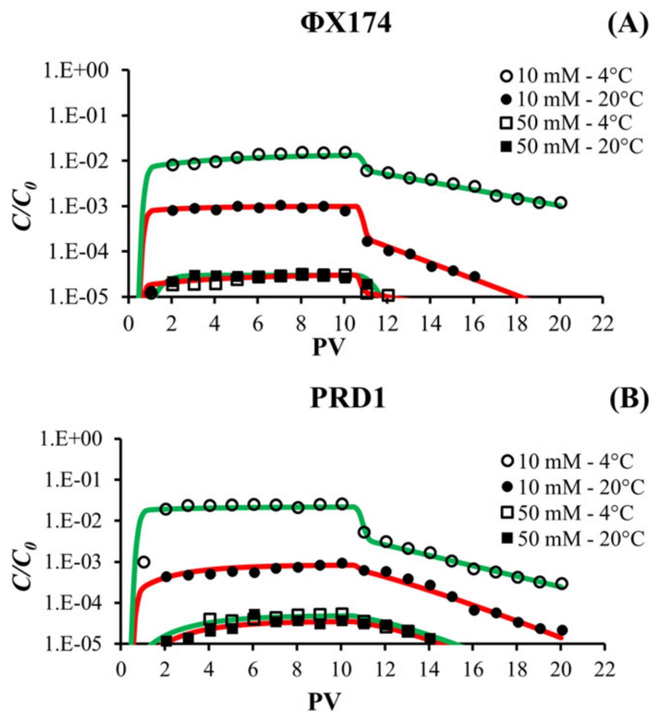

Fig. 1. Observed effluent concentrations (marker) and corresponding model fits (solid line) for representative effluent concentrations of viruses (A) ΦX174 and (B) PRD1 for experiments conducted at temperature = 4 and 20 °C, IS = 10 and 50 mM Na^+ and pore water velocity = 0.1 m day^{-1}. Table 2 provides the values of fitted parameters (k_{att1}, k_{att2} and k_{det2}). The BTCs showed negligible virus retention when the viruses were suspended in a solution with IS = 1 mM (mass balance data is presented in Table S3).

parameters. Values of k_{att1} were found to be more than one order of magnitude greater than those of k_{att2} ($p < 0.0007$) and, therefore, interaction with site 1 accounted for almost 100% of the virus retention (see Table 2). Hence, the values of k_{att1} were used to compare the kinetics of virus attachment at various conditions. Table 2 shows that the average value of k_{att1} for both viruses increased with IS, suggesting that electrostatics dominated virus attachment. The average value of k_{att} for ΦX174 was regularly greater than those of PRD1 over the range of IS, consistent with the isoelectric point value of 6.6 for ΦX174 compared with that of 3.4 for PRD1 (Sasidharan et al., 2016). Similar to the observed BTCs, values of k_{att1} only showed a significant sensitivity ($p < 0.0001$) to temperature when the IS was 10 mM. Specifically, the average values of k_{att1} at 20 °C were 80 and 109% significantly ($p < 0.0002$) higher than those at 4 °C for ΦX174 and PRD1, respectively. Our experimental observations were consistent with previous studies (Chrysikopoulos and Aravantinou, 2014; Gharabaghi et al., 2015; Kim and Walker, 2009; McCaulou et al., 1995). For example, (Kim and Walker, 2009) reported that the k_{att} value for latex microspheres increased by 173% when the temperature increased from 10 to 25 °C. Values of η are presented in Table 2 to show the contribution of temperature on mass transfer. It is observed that the increase in temperature from 4 to 20 °C resulted in an increase in η by only ~8–12% (Table 2). This increase in η with temperature, therefore, cannot fully explain the observed increase in the value of k_{att1} (80–109%) when the IS = 10 mM. As a result, it is concluded that the value of α should have also increased with temperature. Indeed, Eq. (4) predicts that α increased by ~47 and 117% for ΦX174 and PRD1, respectively, when the temperature increased from 4 to 20 °C. This substantial increase in α at higher temperature suggests that the probability of overcoming the energy barrier was higher for viruses when the temperature increased from 4 to 20 °C. It should be mentioned that the survival test of viruses at the experimental conditions and duration confirmed a stable virus concentration (i.e., negligible inactivation, Fig. S1). There was a slight difference between the measured virus concentration between the 4 and 20 °C but the difference was < 0.02 log. Therefore, it is confirmed that the observed enhanced retention was due to the influence of temperature on k_{att} rather than on inactivation rate coefficient.

In order to understand the effect of temperature on the retention of abiotic colloids, additional transport experiments were conducted using the latex NPs (50 and 100 nm) at 4 and 20 °C for various IS and pore water velocity values. Figs. 2 and 3 present the observed and simulated BTCs for these experiments. Tables 3 and S4 provide values of mass percentage of retained particles and replicate information for the latex NPs experiments, respectively. Similar trends to those of viruses were observed in these experiments, that is, an enhanced latex NP retention was only observed at the higher temperature at intermediate IS conditions (i.e., when the IS was 10 and 30 mM). Comparison of Figs. 2 and 3 at the IS of 10 and 30 mM and the corresponding values of PR (Table 3) indicates that the relative importance of temperature on particle retention was also a function of the pore water velocity. Results show that the increase in the PR with temperature for the IS of 10 and 30 mM was greater when the pore water velocity was lower. These observations collectively demonstrate a coupled effect of IS, pore water velocity, and temperature on latex NP retention in porous media.

Fitted values of k_{att1}, k_{att2}, S_{max1}, and S_{max2} for the latex NPs under various experimental conditions are presented in Table 3. Note that the values of fitted parameters are not presented when latex NP retention was negligible (IS = 1 mM) or when breakthrough concentrations were below the detection limit (IS = 50 mM). The goodness of fit for the IS of 10 and 30 mM simulations confirmed the assumption of Langmuir blocking on both sites 1 and 2, and negligible detachment. Fitted values of k_{att1} and k_{att2} were not always unique because latex NP concentrations in the initial stage of breakthrough were below the detection limit of our measurement equipment. However, the fitted values of S_{max1} and S_{max2} were unique, as the final values of the fitting process were not affected by the initial values of the parameters. In addition, the Akaike Information Criterion (Akaike, 1974) and R^2 values included in Hydrus-1D indicated that the two-site kinetic model with S_{max1} and S_{max2} provides the best model fit for the observed BTCs. Table 3 presents calculated values of $S_{max} = S_{max1} + S_{max2}$ that were used to calculate S_f (Eq. (5)). It is noted that only a small fraction of the sand surface

Table 2
Experimental conditions and the values of fitted parameters for viruses.

Virus	Temperature	IS	Pore water velocity	Mass retained	k_{att1}	Percentage increase of k_{att1}	k_{att2}	k_{det2}	R^2	η	Percentage increase of η	α	Percentage increase of α
	[°C]	[mM]	[m day^{-1}]	[log]	[day^{-1}]	[%]	[day^{-1}]	[day^{-1}]	[%]		[%]		[%]
ΦX174	20	10	0.1	3.3	16 ± 0.7	80.8	0.5 ± 0.09	0.9 ± 0.03	78.3	0.71	8.3	0.07	47.1
	4			1.8	9 ± 0.2		1.6 ± 0.02	0.5 ± 0.05	74.1	0.65		0.05	
	20	50	0.1	4.7	25 ± 0.2	0.63	1.6 ± 0.2	1.4 ± 0.4	87.1	0.71	8.3	0.11	0
	4			4.7	25 ± 0.1		1.7 ± 0.03	0.5 ± 0.04	80.4	0.65		0.11	
PRD1	20	10	0.1	3.1	17 ± 0.3	109.7	3.8 ± 0.09	1.4 ± 0.08	80.2	0.60	12.4	0.10	117.4
	4			1.3	8 ± 0.2		0.4 ± 0.03	0.6 ± 0.04	83.4	0.54		0.04	
	20	50	0.1	4.6	24 ± 0.7	3.9	9.2 ± 0.03	2.3 ± 0.01	82.7	0.60	12.4	0.16	0
	4			4.6	23 ± 0.8		7.9 ± 0.09	2.1 ± 0.01	84.4	0.54		0.16	

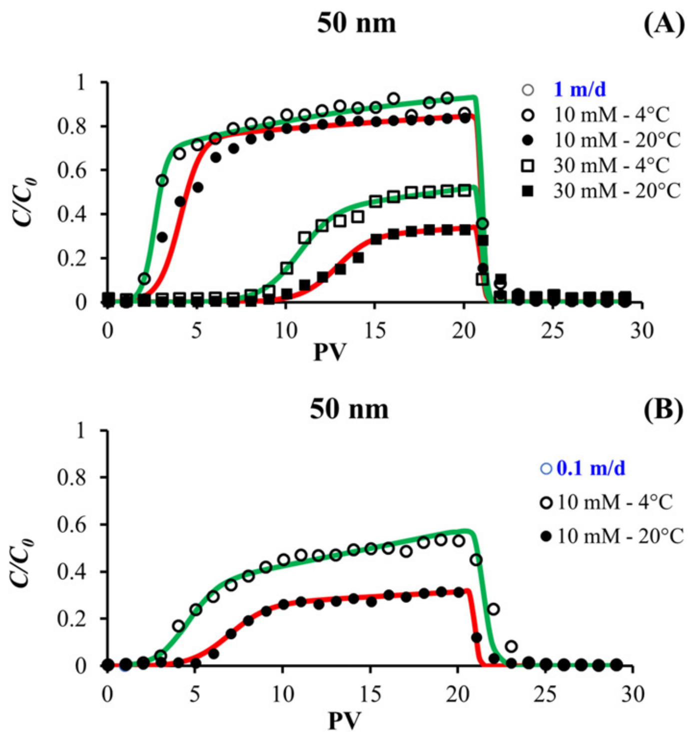

Fig. 2. Observed effluent concentrations (marker) and corresponding model fits (solid line) for representative effluent concentrations of 50 nm latex NPs for experiments conducted at pore water velocity of (A) 1 m day^{-1} and (B) 0.1 m day^{-1}, temperature = 4 and 20 °C, and IS = 10 and 30 mM Na^{+} and Table 3 provides the values of fitted parameters (k_{att1}, k_{att2} and S_{max}).

contributed to latex NP attachment when the IS was 10 and 30 mM (< 33.4%). Note that increasing IS and temperature and decreasing NP size and pore water velocity increased the value of S_f. Interestingly, values of S_f were observed to increase significantly ($p < 0.002$) by ~ 44–160% at the IS of 10 and 30 mM when the temperature increased from 4 to 20 °C.

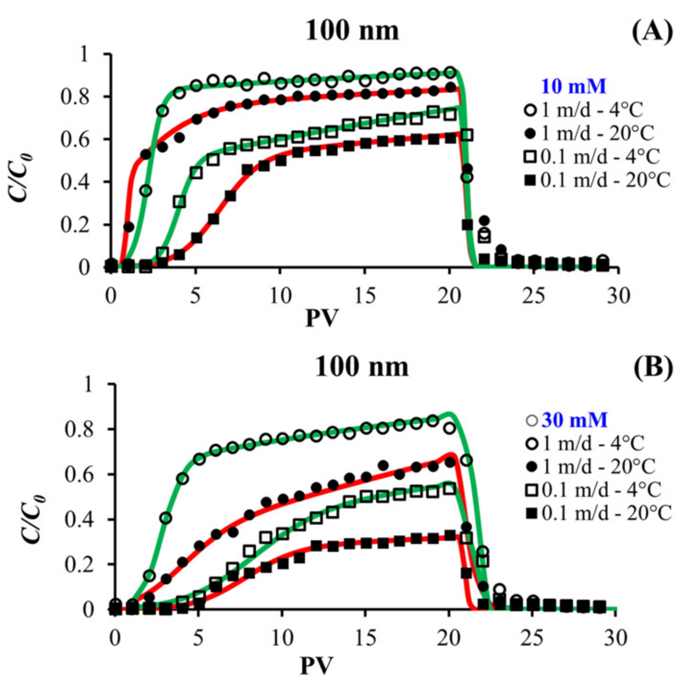

Fig. 3. Observed effluent concentrations (marker) and corresponding model fits (solid line) for representative effluent concentrations of 100 nm latex NPs for experiments conducted at IS (A) 10 mM and (B) 30 mM Na^{+}, temperature = 4 and 20 °C, and pore water velocity = 0.1 and 1 m day^{-1}. Table 3 provides the values of fitted parameters (k_{att1}, k_{att2} and S_{max}).

The fitted BTCs of NPs showed a bimodal shape. In particular, the BTCs were initially delayed, next they rapidly increased, and then slowly approached the influent particle concentration. The initial delay was increased with increasing IS and temperature. An explanation for the dependence of latex NP retention on IS and flow velocity and the need to use the two-site kinetic model with a Langmuirian blocking function for each site was previously provided by (Sasidharan et al., 2014).

4.3. XDLVO interaction energy for a chemically and physically heterogeneous surface

Recall that XDLVO calculations for viruses and latex NPs interacting with a homogeneous sand surface predicted a large $\Delta\Phi_a$ (>7 kT) and negligible attachment when the IS was 1, 10, and 30 mM (Table 1). Natural sand surfaces always exhibit some degree of heterogeneity at the nanoscale. For example, Fig. S2 shows the presence of micro-nanoscale surface roughness on a river sand grain observed under scanning electron microscopy (Quanta 450, Adelaide microscopy, The University of Adelaide, Australia). Similarly, Han et al. (2016) measured the surface roughness of bare quartz sand using atomic force microscopy and reported that the average surface roughness was ~33.4 nm. Nanoscale surface physical heterogeneities (roughness) and chemical heterogeneity (mineral defects, isomorphic substitutions, adsorption of different ions, organic, and/or metal oxides) have been considered in XDLVO calculations to account for observed attachment under unfavorable conditions (Bradford and Torkzaban, 2012; Bradford and Torkzaban, 2013; Hoek et al., 2003; Huang et al., 2009; Shen et al., 2012). Additional XDLVO calculations on physically and chemically heterogeneous sand were, therefore, conducted in an attempt to explain the observed temperature dependency of virus and latex NP retention. We acknowledge that the virus exhibits chemical (protein coat and lipid membrane) (Meder et al., 2013) and physical heterogeneity (spikes) (Huiskonen et al., 2007; Kazumori, 1981) on their surface but this has been not characterized very well. Similar to many previous studies, we therefore only consider XDLVO calculations on a hypothetical solid-water-interface (Castro and Tufenkji, 2007; Loveland et al., 1996; Wong et al., 2014).

Table 3
Experimental conditions, percentage of mass retained (PR) and values of fitted parameters for 50 and 100 nm latex NPs.

NP [nm]	Temperature [°C]	IS [mM]	Pore water velocity [m day^{-1}]	PR [%]	k_{att1} [day^{-1}]	k_{att2} [day^{-1}]	S_{max} [No kg^{-1}]	R^2 [%]	S_f [%]	Percentage increase of S_f [%]	η	Percentage increase of η [%]
50	20	10	1	33 ± 3.2	123 ± 0.4	6 ± 0.2	2.7×10^{14}	99.7	5.1	108.5	0.30	25.1
	4			23 ± 1.9	122 ± 0.7	8 ± 0.1	1.3×10^{14}	99.5	2.4		0.24	
	20	10	0.1	79 ± 1.5	19 ± 0.4	2 ± 0.8	1.8×10^{15}	99.8	33.4	159.6	0.63	11.1
	4			59 ± 2.1	8 ± 0.2	1 ± 0.9	7.0×10^{14}	95.2	12.9		0.57	
	20	30	1	84 ± 3.9	442 ± 0.5	27 ± 0.9	1.0×10^{15}	95.6	19.0	44.4	0.30	25.1
	4			75 ± 3.1	291 ± 0.1	21 ± 0.3	7.1×10^{14}	99.4	13.2		0.24	
100	20	10	1	23 ± 1.8	11 ± 0.1	5 ± 0.7	6.7×10^{13}	98.7	4.9	115.8	0.22	28.5
	4			16 ± 1.4	66 ± 0.3	3 ± 0.8	3.1×10^{13}	93.7	2.3		0.17	
	20	10	0.1	58 ± 4.1	11 ± 0.4	1 ± 0.4	1.6×10^{14}	99.3	11.7	96.9	0.54	15.0
	4			43 ± 3.2	14 ± 0.9	1 ± 0.4	8.0×10^{13}	97.8	5.9		0.47	
	20	30	1	53 ± 1.8	49 ± 0.6	22 ± 0.8	8.8×10^{13}	98.7	6.5	55.7	0.22	28.5
	4			25 ± 2.5	67 ± 0.9	8 ± 0.9	5.7×10^{13}	99.7	4.2		0.17	
	20	30	0.1	79 ± 3.9	14 ± 0.3	2 ± 0.7	2.5×10^{14}	98.4	18.5	48.9	0.54	15.0
	4			66 ± 2.8	12 ± 0.2	1 ± 0.9	1.7×10^{14}	97.8	12.4		0.47	

Previous studies have demonstrated that roughness height (h_r), roughness fraction (f_r), positive zeta potential (ζ_+), and positive zeta potential fraction (f_+) at a particular location on the collector surface can have a significant influence on the magnitude of $\Delta\Phi_a$ (Bradford and Torkzaban, 2013; Torkzaban and Bradford, 2016). The values of $\Delta\Phi_a$ calculated for viruses and latex NPs interacting with a chemically and physically heterogeneous sand surface for all the IS and the two temperatures are given in Table 1. Specific heterogeneity parameter values used in these calculations included $f_r = 0.05$, $h_r = 20$ nm, $f_+ = 0.1$ and $\zeta_+ = 1$ mV. The magnitude of $\Delta\Phi_a$ was significantly reduced ($p < 0.0002$) for the heterogeneous surface compared to the homogeneous surface (Table 1). For example, Table 1 shows that the value of $\Delta\Phi_a$ for the PRD1 virus at IS = 10 mM decreased from 28 and 24 kT on the homogeneous surface to 1.3 and 1.1 kT on the heterogeneous surface at 4 and 20 °C, respectively.

Temperature had a relatively minor (<3 kT) influence on $\Delta\Phi_a$ in comparison to physical and chemical heterogeneity. Nevertheless, the Maxwellian kinetic energy model predicts that a small reduction in $\Delta\Phi_a$ can significantly increase the probability for particles to attach in a primary minimum when $\Delta\Phi_a$ < 7 kT (Torkzaban and Bradford, 2016). Consequently, the increase in attachment (k_{att} and S_f) with an increase in temperature depends on the overall value of $\Delta\Phi_a$. Temperature variations did not have a significant influence on the attachment when the IS = 1 mM because the value of $\Delta\Phi_a$ was >11 kT even on a nanoscale heterogeneous surface and this always produced unfavorable attachment conditions. Similarly, the influence of temperature on attachment was also not important when the IS = 50 mM. In this case, $\Delta\Phi_a$ was nearly completely eliminated for both latex NPs and viruses on both homogeneous and nanoscale heterogeneous surfaces. In contrast, temperature had a large influence on attachment (k_{att} and S_f) at intermediate IS conditions (10 and 30 mM) because small changes in $\Delta\Phi_a$ < 7 kT drastically increased the probability for particles to diffuse over $\Delta\Phi_a$ into the primary minimum.

4.4. Coupled effect of IS, water velocity, and temperature on α and S_f values

Numerical simulations were conducted to better understand the coupled influence of IS and temperature on α and S_f values. The model of (Bradford and Torkzaban, 2015) was employed for this purpose. These simulations considered a homogeneous particle interacting with a physically and chemically heterogeneous collector surface at 10,000 random A_Z locations. The mean values of physical and chemical heterogeneity parameters in these simulations included: $f_+ = 0.1$, $\zeta_+ = 1$ mV, $f_r = 0.1$, $h_r = 20$ nm, and zeta potential values from Table 1. It should be noted that the simulations shown below are a representative example to show the effect of collector surface heterogeneity on α (virus) and S_f (latex NPs) values. Natural surfaces are more complex and determining the accurate heterogeneity parameter distributions is likely to be impossible. Theoretical values of α and S_f were denoted below as α_T and S_{fT}, respectively.

Fig. 4 presents the percentage increase of α_T values for viruses and S_{fT} values for latex NPs as a function of IS when the temperature was increased from 4 to 20 °C. It is observed that the percentage increase of α_T values rapidly increased from a minimum value at IS = 1 mM to a maximum at IS = 10 mM, and then slowly decreased with IS and became negligible at IS ≥40 mM. Similar behavior was observed for the percentage increase of S_{fT} values. These results were consistent with our experimental observations; e.g., an increase in temperature from 4 to 20 °C produced an increase in attachment (α and S_f) when the IS = 10 and 30 mM, but had a negligible influence at IS = 1 and 50 mM. In addition, Fig. 4 and experimental observations (Tables 2 and 3) also indicate that the effect of temperature on attachment was more evident for bigger particles (PRD1 virus or 100 nm latex NP). The larger particles had $\Delta\Phi_a$ values (<7 kT) that were in the range of

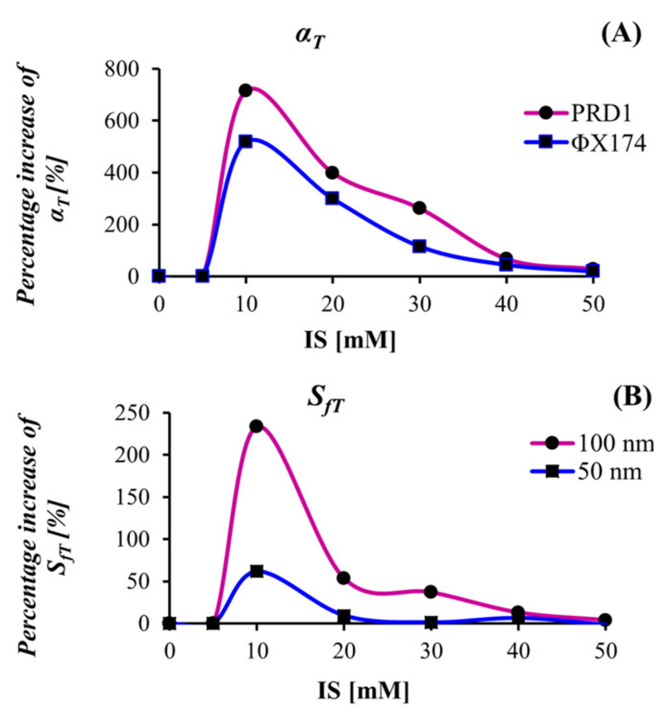

Fig. 4. The percentage increase of (A) theoretical attachment efficiency (α_T) of viruses (PRD1 and ΦX174) and (B) theoretical maximum solid fraction contributed to attachment (S_{fT}) of latex NPs (50 and 100 nm) interacting with a heterogeneous sand surface when the temperature increased from 4 to 20 °C. The mean values of parameters used for the simulations are $f_r = 0.1$, $h_r = 20$ nm, $f_+ = 0.1$ and $\zeta_+ = 1$ mV. Zetapotential values used in the calculations are given in Table 1.

the greatest sensitivity to particle diffusion. A small reduction of $\Delta\Phi_a$ at 20 °C allowed more particles to overcome the shallow energy barrier to attachment in a primary minimum, and substantially enhanced α and S_f.

Figs. 2 and 3 indicate that a decrease in pore water velocity enhanced the retention of latex NPs at a given ionic strength. Experimental and theoretical results have shown that colloidal particles weakly associated with solid surfaces via a shallow secondary minimum may translate over the surface by hydrodynamic forces to reach some locations where the attachment is favorable (Kuznar and Elimelech, 2007; Sasidharan et al., 2014; Torkzaban et al., 2010). Bendersky et al. (2015) reported that Brownian motion is more significant than or comparable to DLVO interactions and hydrodynamic forces for small particles (<200 nm) at low flow velocities. Consequently, it is expected that particles with more residence time on the solid surface due to a lower fluid velocity would have an increased probability to diffuse over a shallow $\Delta\Phi_a$ and become attached in the primary energy minimum (Bendersky et al., 2015).

The data from groundwater sources across the world show that the temperature may range from 4 to 32 °C (Kar et al., 2010; Vanderzalm et al., 2010; Yates et al., 1985). We acknowledge that, only two temperatures that correspond to average groundwater extremes were considered in the laboratory experiments in this study. However, the simulated value of α_T and S_{fT} at various temperatures were consistent with our experimental observation. Fig. S3 shows the percentage increase of α_T for viruses (PRD1 and ΦX174) and S_{fT} for latex NPs (50 and 100 nm) interacting with a heterogeneous sand surface when the temperature increases from 0 to 25 °C as an increment of 5 °C at IS = 10 mM. Results show a systematic nonlinear increase in α_T and S_{fT} with increasing temperature, with greater increases occurring for the larger virus (PRD1) and latex NP (100 nm).

5. Conclusion

This study showed that an increase in temperature from 4 °C to 20 °C increased the retention of viruses and latex NPs in porous media under intermediate IS (10 and 30 mM) conditions. In particular, the value of k_{att}, α (for the virus), and S_f (for the latex NPs) calculated from fitted model parameters showed an increase up to 109, 117, and 160%, respectively, at intermediate IS conditions. Conversely, temperature had negligible influence on k_{att}, α, and S_f values when IS was 1 mM or 50 mM. These results could not be explained by differences in η with temperature. An explanation was obtained from XDLVO calculations on sand surfaces that included nanoscale roughness and chemical heterogeneity. The temperature had a relatively minor (<3 kT) influence on the magnitude $\Delta\Phi_a$ in comparison to physical and chemical heterogeneity. However, a small reduction in $\Delta\Phi_a$ at a higher temperature significantly increased the probability for particles to attach in the primary minimum under intermediate IS conditions. Numerical model predictions conducted to understand the coupled effect of IS, temperature, and colloid size were consistent with the experimental observation.

The experiments presented here were conducted in a simple electrolyte solution at pH 5.5–5.8 and using a clean quartz sand. Whereas, natural groundwater can have different chemical compositions (presence of mono or divalent ions, high pH, and/or organic matter) and aquifer sediment can have various mineral properties, clay fractions, and/or grain size distributions. Ongoing research in our laboratory aims at extending this work to examine the transport of viruses and NPs in aquifer sediments and ground water over a wide range of environmentally relevant conditions. A better understanding of the effect of temperature on pathogen and engineered NP transport has significant implications for management of potential health and environmental risks associated with groundwater and water reuse. Surface water-groundwater mixing via recharge and seasonal changes in water temperature may significantly affect virus and NP attachment to porous media. Drinking water produced by domestic wells in cold climate regions might be at a higher risk of virus and NP contaminant exposure. Therefore, the influence of temperature should be considered in predictive models in order to accurately assess risks of groundwater contamination.

Notes

The authors declare no competing financial interest.

Funding

Funding for this research was provided by the National Centre for Groundwater Research and Training, an Australian Government initiative, supported by the Australian Research Council and the National Water Commission, and by CSIRO Land and Water program.

Acknowledgements

The work was conducted in the CSIRO Laboratories at the Waite Campus, Adelaide, South Australia. We thank Mr. Harold Rankine for assisting in conducting laboratory experiments and Mr. Toney Hirnyk for equipment maintenance support. We also thank Prof. Patrick Hesp (Flinders University, Adelaide), Dr. Joanne Vanderzalm (CSIRO, Adelaide) and external reviewers who have contributed ideas and suggestions to improve this manuscript.

Appendix A. Supplementary data

Supplementary data to this article can be found online at http://dx.doi.org/10.1016/j.jconhyd.2016.11.004.

References

ISO 10705-2-2000, 2000. ISO 10705-2-2000 Water Quality - Detection and Enumeration of Bacteriophages - Part 2 - Enumeration of Somatic Coliphages. I.O.f. Standardisation (Geneva, Switzerland).

Adamczyk, Z., 2006. Particles at Interfaces: Interactions, Deposition, Structure. 9. Academic Press.

Adamczyk, Z., Nattich-Rak, M., Sadowska, M., Michna, A., Szczepaniak, K., 2013. Mechanisms of nanoparticle and bioparticle deposition - kinetic aspects. Colloids Surf. A Physicochem. Eng. Asp. 439, 3–22.

Akaike, H., 1974. A new look at the statistical model identification. IEEE Trans. Autom. Control 19 (6), 716–723.

Argent, J., et al., 2015. Visualization of micro-particle retention on a heterogeneous surface using micro-models: influence of nanoscale surface roughness. Transp. Porous Media 1–15.

Attinti, R., Wei, J., Kniel, K., Sims, J.T., Jin, Y., 2010. Virus' (MS2, ϕX174, and Aichi) attachment on sand measured by atomic force microscopy and their transport through sand columns. Environ. Sci. Technol. 44 (7), 2426–2432.

Bales, R.C., Hinkle, S.R., Kroeger, T.W., Stocking, K., Gerba, C.P., 1991. Bacteriophage adsorption during transport through porous media: chemical perturbations and reversibility. Environ. Sci. Technol. 25 (12), 2088–2095.

Bellamy, W.D., Hendricks, D.W., Logsdon, G.S., 1985. Slow sand filtration: influences of selected process variables. J. Am. Water Works Assoc. 77 (12), 62–66.

Bendersky, M., Santore, M.M., Davis, J.M., 2015. The Effects of Brownian Motion on Particle Interactions With Patchy Surfaces Bearing Nanoscale Features (arXiv preprint arXiv: 1510.06484).

Bhattacharjee, S., Ko, C.H., Elimelech, M., 1998. DLVO interaction between rough surfaces. Langmuir 14 (12), 3365–3375.

Bhattacharjee, S., Chen, J.Y., Elimelech, M., 2000. DLVO interaction energy between spheroidal particles and a flat surface. Colloids Surf. A Physicochem. Eng. Asp. 165 (1–3), 143–156.

Bradford, S.A., Kim, H., 2012. Causes and implications of colloid and microorganism retention hysteresis. J. Contam. Hydrol. 138-139, 83–92.

Bradford, S.A., Torkzaban, S., 2012. Colloid adhesive parameters for chemically heterogeneous porous media. Langmuir 28 (38), 13643–13651.

Bradford, S.A., Torkzaban, S., 2013. Colloid interaction energies for physically and chemically heterogeneous porous media. Langmuir 29 (11), 3668–3676.

Bradford, S.A., Torkzaban, S., 2015. Determining parameters and mechanisms of colloid retention and release in porous media. Langmuir 31 (44), 12096–12105.

Bradford, S.A., Bettahar, M., Simunek, J., van Genuchten, M.T., 2004. Straining and attachment of colloids in physically heterogeneous porous media. Vadose Zone J. 3 (2), 384–394.

Bradford, S.A., Tadassa, Y.F., Jin, Y., 2006. Transport of coliphage in the presence and absence of manure suspension. J. Environ. Qual. 35 (5), 1692–1701.

Bradford, S.A., Torkzaban, S., Kim, H., Simunek, J., 2012. Modeling colloid and microorganism transport and release with transients in solution ionic strength. Water Resour. Res. 48 (9) (n/a–n/a).

Castro, F.D., Tufenkji, N., 2007. Relevance of nontoxigenic strains as surrogates for *Escherichia coli* O157:H7 in groundwater contamination potential: role of temperature and cell acclimation time. Environ. Sci. Technol. 41 (12), 4332–4338.

Chrysikopoulos, C.V., Aravantinou, A.F., 2012. Virus inactivation in the presence of quartz sand under static and dynamic batch conditions at different temperatures. J. Hazard. Mater. 233–234, 148–157.

Chrysikopoulos, C.V., Aravantinou, A.F., 2014. Virus attachment onto quartz sand: role of grain size and temperature. J. Environ. Chem. Eng. 2 (2), 796–801.

Chu, Y., Jin, Y., Flury, M., Yates, M.V., 2001. Mechanisms of virus removal during transport in unsaturated porous media. Water Resour. Res. 37 (2), 253–263.

Da Silva, A.K., Kavanagh, O.V., Estes, M.K., Elimelech, M., 2011. Adsorption and aggregation properties of norovirus GI and GII virus-like particles demonstrate differing responses to solution chemistry. Environ. Sci. Technol. 45 (2), 520–526.

Derjaguin, B.V., 1941. Theory of the stability of strongly charged lyophobic sols and the adhesion of strongly charged particles in solutions of electrolytes. Acta Physicochim. 14, 633–662.

Dhont, J.K.G., Briels, W.J., 2008. Single-particle thermal diffusion of charged colloids: double-layer theory in a temperature gradient. Eur. Phys. J. E 25 (1), 61–76.

Elimelech, M., Chen, W.H., Waypa, J.J., 1994. Measuring the zeta (electrokinetic) potential of reverse osmosis membranes by a streaming potential analyzer. Desalination 95 (3), 269–286.

Fang, J., Xu, M.J., Wang, D.J., Wen, B., Han, J.Y., 2013. Modeling the transport of TiO2 nanoparticle aggregates in saturated and unsaturated granular media: effects of ionic strength and pH. Water Res. 47 (3), 1399–1408.

Fletcher, M., 1977. The effects of culture concentration and age, time, and temperature on bacterial attachment to polystyrene. Can. J. Microbiol. 23 (1), 1–6.

Freitas, C., Müller, R.H., 1998. Effect of light and temperature on zeta potential and physical stability in solid lipid nanoparticle (SLN™) dispersions. Int. J. Pharm. 168 (2), 221–229.

Galisteo, F., de las Nieves López, F.J., Cabrerizo, M., Hidalgo-Alvarez, R., 1990. Effects of particle concentration, ionic strength, pH and temperature on the microelectrophoretic mobility of cationic polystyrene latex. I. In: Lindman, B., Rosenholm, J.B., Stenius, P. (Eds.), Surfactants and Macromolecules: Self-assembly at Interfaces and in Bulk. Progress in Colloid & Polymer Science, pp. 313–320 (Steinkopff).

Gallardo-Moreno, A.M., et al., 2003. Influence of the growth medium, suspending liquid and measurement temperature on the physico-chemical surface properties of two enterococci strains. J. Adhes. Sci. Technol. 17 (14), 1877–1887.

García-García, S., Jonsson, M., Wold, S., 2006. Temperature effect on the stability of bentonite colloids in water. J. Colloid Interface Sci. 298 (2), 694–705.

García-García, S., Wold, S., Jonsson, M., 2009. Effects of temperature on the stability of colloidal montmorillonite particles at different pH and ionic strength. Appl. Clay Sci. 43 (1), 21–26.

Gharabaghi, B., et al., 2015. Temperature effect on the transport of bromide and *E. coli* NAR in saturated soils. J. Hydrol. 522, 418–427.

Gregory, J., 1981. Approximate expressions for retarded van der Waals interaction. J. Colloid Interface Sci. 83 (1), 138–145.

Gutierrez, L., Mylon, S.E., Nash, B., Nguyen, T.H., 2010. Deposition and aggregation kinetics of rotavirus in divalent cation solutions. Environ. Sci. Technol. 44 (12), 4552–4557.

Han, Y., et al., 2016. Transport, retention, and long-term release behavior of ZnO nanoparticle aggregates in saturated quartz sand: Role of solution pH and biofilm coating. Water Res. 90, 247–257.

Hendricks, D.W., Post, F.J., Khairnar, D.R., 1979. Adsorption of bacteria on soils: experiments, thermodynamic rationale, and application. Water Air Soil Pollut. 12 (2), 219–232.

Hijnen, W.A., Brouwer-Hanzens, A.J., Charles, K.J., Medema, G.J., 2005. Transport of MS2 phage, *Escherichia coli*, *Clostridium perfringens*, *Cryptosporidium parvum*, and *Giardia intestinalis* in a gravel and a sandy soil. Environ. Sci. Technol. 39 (20), 7860–7868.

Hoek, E.M.V., Bhattacharjee, S., Elimelech, M., 2003. Effect of membrane surface roughness on colloid-membrane DLVO interactions. Langmuir 19 (11), 4836–4847.

Hogg, R., Healy, T.W., Fuerstenau, D.W., 1966. Mutual coagulation of colloidal dispersions. Trans. Faraday Soc. 62, 1638–1651.

Huang, X., Bhattacharjee, S., Hoek, E.M.V., 2009. Is surface roughness a "scapegoat" or a primary factor when defining particle–substrate interactions? Langmuir 26 (4), 2528–2537.

Huiskonen, J.T., Manole, V., Butcher, S.J., 2007. Tale of two spikes in bacteriophage PRD1. Proc. Natl. Acad. Sci. 104 (16), 6666–6671.

IBM SPSS [computer software] IBM Corp. Released, 2013. IBM SPSS Statistics for Windows, Version 22.0. IBM Corp., Armonk, NY.

Ishido, T., Mizutani, H., Baba, K., 1983. Streaming potential observations, using geothermal wells and in situ electrokinetic coupling coefficients under high temperature. Tectonophysics 91 (1), 89–104.

Johnson, P.R., Elimelech, M., 1995. Dynamics of colloid deposition in porous media: blocking based on random sequential adsorption. Langmuir 11 (3), 801–812.

Johnson, P.R., Sun, N., Elimelech, M., 1996. Colloid transport in geochemically heterogeneous porous media: modeling and measurements. Environ. Sci. Technol. 30 (11), 3284–3293.

Kar, S., et al., 2010. Arsenic-enriched aquifers: occurrences and mobilization of arsenic in groundwater of Ganges Delta Plain, Barasat, West Bengal, India. Appl. Geochem. 25 (12), 1805–1814.

Kazumori, Y., 1981. Electron microscopic studies of bacteriophage φ X174 intact and 'eclipsing' particles, and the genome by the staining and shadowing method. J. Virol. Methods 2 (3), 159–167.

Kim, H.N., Walker, S.L., 2009. *Escherichia coli* transport in porous media: influence of cell strain, solution chemistry, and temperature. Colloids Surf. B: Biointerfaces 71 (1), 160–167.

Kim, H.N., Bradford, S.A., Walker, S.L., 2009. *Escherichia coli* O157:H7 transport in saturated porous media: role of solution chemistry and surface macromolecules. Environ. Sci. Technol. 43 (12), 4340–4347.

Kuznar, Z.A., Elimelech, M., 2007. Direct microscopic observation of particle deposition in porous media: role of the secondary energy minimum. Colloids Surf. A Physicochem. Eng. Asp. 294 (1–3), 156–162.

Logan, B.E., Jewett, D.G., Arnold, R.G., Bouwer, E.J., O'Melia, C.R., 1995. Clarification of clean-bed filtration models. J. Environ. Eng. 121 (12), 869–873.

Loveland, J.P., Ryan, J.N., Amy, G.L., Harvey, R.W., 1996. The reversibility of virus attachment to mineral surfaces. Colloids Surf. A Physicochem. Eng. Asp. 107, 205–221.

Ma, H., Hradisky, M., Johnson, W.P., 2013. Extending applicability of correlation equations to predict colloidal retention in porous media at low fluid velocity. Environ. Sci. Technol. 47 (5), 2272–2278.

Magal, E., Weisbrod, N., Yechieli, Y., Walker, S.L., Yakirevich, A., 2011. Colloid transport in porous media: impact of hyper-saline solutions. Water Res. 45 (11), 3521–3532.

Malvern Instruments Ltd., 2004. Zetasizer Nano Series User Manual. Malvern Instruments Ltd., United Kingdom.

McCaulou, D.R., Bales, R.C., Arnold, R.G., 1995. Effect of temperature controlled motility on transport of bacteria and microspheres through saturated sediment. Water Resour. Res. 31 (2), 271–280.

Meder, F., et al., 2013. The role of surface functionalization of colloidal alumina particles on their controlled interactions with viruses. Biomaterials 34 (17), 4203–4213.

Messina, F., Marchisio, D.L., Sethi, R., 2015. An extended and total flux normalized correlation equation for predicting single-collector efficiency. J. Colloid Interface Sci. 446, 185–193.

Rajagopalan, R., Tien, C., 1976. Trajectory analysis of deep-bed filtration with the sphere-in-cell porous media model. AICHE J. 22 (3), 523–533.

Reppert, P.M., Morgan, F.D., 2003. Temperature-dependent streaming potentials: 1. Theory. J. Geophys. Res. Solid Earth 108 (B11) (n/a–n/a).

Rodríguez, K., Araujo, M., 2006. Temperature and pressure effects on zeta potential values of reservoir minerals. J. Colloid Interface Sci. 300 (2), 788–794.

Ruckenstein, E., Prieve, D.C., 1976. Adsorption and desorption of particles and their chromatographic separation. AICHE J. 22 (2), 276–283.

Ryan, J.N., Elimelech, M., Ard, R.A., Harvey, R.W., Johnson, P.R., 1999. Bacteriophage PRD1 and silica colloid transport and recovery in an iron oxide-coated sand aquifer. Environ. Sci. Technol. 33 (1), 63–73.

Sadeghi, G., et al., 2011. Systematic study of effects of pH and ionic strength on attachment of phage PRD1. Ground Water 49 (1), 12–19.

Sadeghi, G., Behrends, T., Schijven, J.F., Hassanizadeh, S.M., 2013. Effect of dissolved calcium on the removal of bacteriophage PRD1 during soil passage: the role of double-layer interactions. J. Contam. Hydrol. 144 (1), 78–87.

Sasidharan, S., Torkzaban, S., Bradford, S.A., Dillon, P.J., Cook, P.G., 2014. Coupled effects of hydrodynamic and solution chemistry on long-term nanoparticle transport and deposition in saturated porous media. Colloids Surf. A Physicochem. Eng. Asp. 457 (0), 169–179.

Sasidharan, S., et al., 2016. Transport and retention of bacteria and viruses in biochar-amended sand. Sci. Total Environ. 548–549, 100–109.

Schijven, J.F., Hassanizadeh, S.M., 2000. Removal of viruses by soil passage: overview of modeling, processes, and parameters. Crit. Rev. Environ. Sci. Technol. 30 (1), 49–127.

Shen, C., Li, B., Huang, Y., Jin, Y., 2007. Kinetics of coupled primary- and secondary-minimum deposition of colloids under unfavorable chemical conditions. Environ. Sci. Technol. 41 (20), 6976–6982.

Shen, C., Huang, Y., Li, B., Jin, Y., 2010. Predicting attachment efficiency of colloid deposition under unfavorable attachment conditions. Water Resour. Res. 46 (11) (n/a-n/a).

Shen, C., et al., 2012. Application of DLVO energy map to evaluate interactions between spherical colloids and rough surfaces. Langmuir 28 (41), 14681–14692.

Sikora, A., Shard, A.G., Minelli, C., 2016. Size and zeta-potential measurement of silica nanoparticles in serum using tunable resistive pulse sensing. Langmuir 32 (9), 2216–2224.

Simunek, J., van Genuchten, M.Th, Sejna, M., 2005. The HYDRUS-1D software package for simulating the one-dimensional movement of water, heat, and multiple solutes in variably-saturated media – version 3.0. HYDRUS Software Series 1 2005. Department of Environmental Sciences, University of California Riverside, Riverside, CA, p. 270.

Sirivithayapakorn, S., Keller, A., 2003. Transport of colloids in unsaturated porous media: a pore-scale observation of processes during the dissolution of air-water interface. Water Resour. Res. 39 (12) (n/a–n/a).

Subrahmanyam, T., Monte, M., Middea, A., Valdiviezo, E., Lins, F., 1999. Contact angles of quartz by capillary penetration of liquids and captive bubble techniques. Miner. Eng. 12 (11), 1347–1357.

Suresh, L., Walz, J.Y., 1997. Direct measurement of the effect of surface roughness on the colloidal forces between a particle and flat plate. J. Colloid Interface Sci. 196 (2), 177–190.

Torkzaban, S., Bradford, S.A., 2016. Critical role of surface roughness on colloid retention and release in porous media. Water Res. 88, 274–284.

Torkzaban, S., Hassanizadeh, S.M., Schijven, J.F., De Bruin, H.A.M., De Roda Husman, A.M., 2006. Virus transport in saturated and unsaturated sand columns. Vadose Zone J. 5 (3), 877–885.

Torkzaban, S., Kim, Y., Mulvihill, M., Wan, J., Tokunaga, T.K., 2010. Transport and deposition of functionalized CdTe nanoparticles in saturated porous media. J. Contam. Hydrol. 118 (3–4), 208–217.

Torkzaban, S., Bradford, S.A., Wan, J., Tokunaga, T., Masoudih, A., 2013. Release of quantum dot nanoparticles in porous media: role of cation exchange and aging time. Environ. Sci. Technol. 47 (20), 11528–11536.

Treumann, S., Torkzaban, S., Bradford, S.A., Visalakshan, R.M., Page, D., 2014. An explanation for differences in the process of colloid adsorption in batch and column studies. J. Contam. Hydrol. 164, 219–229.

Tufenkji, N., Elimelech, M., 2004. Correlation equation for predicting single-collector efficiency in physicochemical filtration in saturated porous media. Environ. Sci. Technol. 38 (2), 529–536.
Tufenkji, N., Elimelech, M., 2005. Breakdown of colloid filtration theory: role of the secondary energy minimum and surface charge heterogeneities. Langmuir 21 (3), 841–852.
USGS, 2013. General interest publications of the U.S. geological survey. U.S. Geological Survey. USGS Office of Ground Water.
Van Oss, C., 1993. Acid—base interfacial interactions in aqueous media. Colloids Surf. A Physicochem. Eng. Asp. 78, 1–49.
Van Oss, C., Chaudhury, M., Good, R., 1988. Interfacial Lifshitz-van der Waals and polar interactions in macroscopic systems. Chem. Rev. 88 (6), 927–941.
Vanderzalm, J.L., Page, D.W., Barry, K.E., Dillon, P.J., 2010. A comparison of the geochemical response to different managed aquifer recharge operations for injection of urban stormwater in a carbonate aquifer. Appl. Geochem. 25 (9), 1350–1360.
Verwey, E.J.W., 1947. Theory of the stability of lyophobic colloids. J. Phys. Colloid Chem. 51 (3), 631–636.
Vogler, E.A., 1998. Structure and reactivity of water at biomaterial surfaces. Adv. Colloid Interf. Sci. 74 (1–3), 69–117.
Wiesner, M.R., Lowry, G.V., Alvarez, P., Dionysiou, D., Biswas, P., 2006. Assessing the risks of manufactured nanomaterials. Environ. Sci. Technol. 40 (14), 4336–4345.
Wong, K., Bouchard, D., Molina, M., 2014. Relative transport of human adenovirus and MS2 in porous media. Colloids Surf. B: Biointerfaces 122, 778–784.
Yan, Z., Huang, X., Yang, C., 2015. Deposition of colloidal particles in a microchannel at elevated temperatures. Microfluid. Nanofluid. 18 (3), 403–414.
Yao, K.-M., Habibian, M.T., O'Melia, C.R., 1971. Water and waste water filtration. Concepts and applications. Environ. Sci. Technol. 5 (11), 1105–1112.
Yates, M.V., Gerba, C.P., Kelley, L.M., 1985. Virus persistence in groundwater. Appl. Environ. Microbiol. 49 (4), 778–781.
Yoon, R.-H., Flinn, D.H., Rabinovich, Y.I., 1997. Hydrophobic interactions between dissimilar surfaces. J. Colloid Interface Sci. 185 (2), 363–370.
You, Y., Han, J., Chiu, P.C., Jin, Y., 2005. Removal and inactivation of waterborne viruses using zerovalent iron. Environ. Sci. Technol. 39 (23), 9263–9269.
Zhang, L., Seagren, E.A., Davis, A.P., Karns, J.S., 2012. Effects of temperature on bacterial transport and destruction in bioretention media: field and laboratory evaluations. Water Environ. Res. 84 (6), 485–496.